

# Fabrication of Nb/Al(AIO $x$ )/Nb DC SQUID by focused ion beam sculpturing

D. Yuvaraj, Gil Bachar, Oren Suchoi, Oleg Shtempluck, and Eyal Buks\*

*Department of Electrical Engineering, Technion Israel Institute of Technology, Haifa 32000, Israel*

(Dated: August 23, 2018)

Highly reproducible Nb/Al(AIO $x$ )/Nb Josephson junction based direct current superconducting quantum interference devices (DC SQUID) were fabricated by three dimensional etching using focused ion beam. Hysteretic and non-hysteretic DC SQUID with critical current ranging from 25 to 1100  $\mu$ A were fabricated by varying the Al barrier and oxygen exposure time. The fabricated DC SQUIDS have shown periodic flux dependence with high modulation factor reaching a value of 92% at 4.2 K.

PACS numbers: 85.25.Dq,85.25.-j,81.07.Oj,81.16.Nd,81.16.Rf

Direct current superconducting quantum interference devices (DC SQUIDS) are formed by enclosing two Josephson junction (JJs) in a superconducting loop. They were primarily used as sensitive magnetic flux detectors and as voltage standards, but in recent years demonstration of SQUIDS as nanoscale position sensors, qubit readout and scanning SQUID microscopy has reopened the interest in these devices [1–4]. SQUIDS based on Nb/Al(AIO $x$ )/Nb JJ have relatively high transition temperature ( $T_c$ ), high flux-voltage modulation factor and good thermal recyclability and can be fabricated with a wide range of critical currents ( $I_c$ ) [5]. Traditionally Nb/Al(AIO $x$ )/Nb SQUIDS with size ranging from few to several hundred microns are fabricated in sequence of steps involving several photolithography and anodization processes, and it also requires in-situ etching for the deposition of top Nb electrode [5]. In spite of the superior properties of Nb/Al(AIO $x$ )/Nb SQUIDS, the fact that a multistep-process is needed for device fabrication has limited its popularity.

The advancement in the nanofabrication techniques lead to the realization of nano sized SQUIDS based on Al/AIO $x$ /Al junctions and Nb nanobridges [4, 6]. SQUIDS based on Al/AIO $x$ /Al are fabricated using a single shadow evaporation process, but the relatively low transition temperature of Al limits the range of possible applications [4]. Although the SQUIDS based on the Nb nanobridges have relatively high  $T_c$  and are relatively easy to fabricate, these SQUIDS are highly hysteretic and the nanobridges typically lose their sinusoidal current phase relationship when cooled to very low temperatures [7, 8]. Compared to alternative nanofabrication techniques, focused ion beam (FIB) offers the possibility to etch the samples in 3D [9]. Recently Watanabe *et al.* have demonstrated the application of 3D FIB etching for the fabrication of JJs and single electron transistors (SET) [10, 11].

We report here a process to fabricate Nb/Al(AIO $x$ )/Nb junction based DC SQUIDS using only a single photolithography step and a single 3D

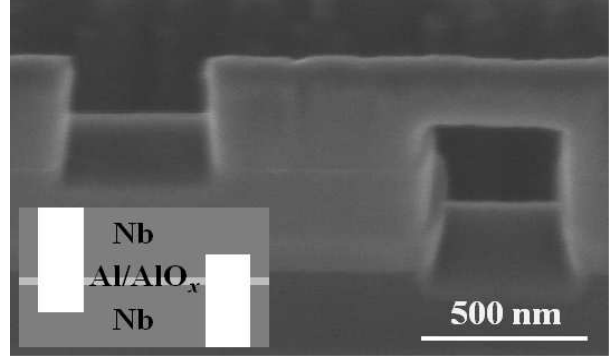


FIG. 1: Scanning electron microscope (SEM) image of the Nb/Al(AIO $x$ )/Nb Josephson Junction (JJ) fabricated by 3D FIB etching. The inset shows a schematic of JJ structure.

FIB etching. Moreover, we present the characteristics of the fabricated hysteretic and non hysteretic DC SQUIDS at low temperature (4.2 K and 0.1 K).

Nb/Al(AIO $x$ )/Nb trilayer was deposited on SiN coated Si substrate at an Ar pressure of  $5 \times 10^{-3}$  mbar at room temperature by DC magnetron sputtering. Thickness of the base and top Nb electrodes was fixed as 350 nm, whereas the thickness of the Al barrier and oxidation conditions were varied for different samples. SQUID loop, magnetic flux line and bonding pads are patterned on the trilayer films using a single photolithography step. The SQUID loop has an area of  $40 \times 40 \mu\text{m}^2$  and the flux lines were fixed 10  $\mu\text{m}$  away from the SQUID loop. JJs in the DC SQUIDS were fabricated using the process similar to the one used by Watanabe *et al.* for the fabrication of trilayer SET [11]. The sample with the trilayer SQUID loop is mounted on wedge shaped ( $45^\circ$ ) sample holder. In the 3D FIB etching process the JJs were fabricated on the arms of the SQUID loop by etching in perpendicular and parallel directions to the sample surface plane. Initially using perpendicular etching with 2.8 nA Ga ion current a 1 micron wide section is formed on each arm of the SQUID loop. The width of these sections is further reduced down to 300 nm using a current of 28 pA. Then JJ's were fabricated on the trilayer bridge by parallel etching, in which the top and the bottom Nb layer

\*Electronic address: eyal@ee.technion.ac.il

Device	Nb/Al/Nb (nm)	$\frac{D}{\text{torr s}}$	$\frac{I_c}{\mu\text{A}}$	$\frac{\Delta I_c}{\mu\text{A}}$	$\frac{J_a}{\text{kA cm}^{-2}}$
DS-A	350/5/350	4.8	750 (H)	25	300
DS-B	350/5/350	4.8	390 (NH)	—	160
DS-C	350/5/350	12	334 (NH)	—	130
DS-D	350/5/350	480	25 (NH)	—	2.4
DS-E	350/3/350	6	1070 (H)	70	450

TABLE I: The parameters of the different DC SQUIDS fabricated using FIB. Device DS-A after anodization process is labeled as device DS-B. The parameter  $D = P\tau$ , where  $P$  is the oxygen partial pressure and  $\tau$  is the oxygen exposure time, characterizes the oxidation dose. In the  $I_c$  column H and NH stands for 'hysteretic' and 'non-hysteretic' respectively. The parameter  $\Delta I_c$  is given by  $\Delta I_c = I_{c1} - I_{c2}$ , where  $I_{c1}$  and  $I_{c2}$  are the critical currents measured in the sweep up and sweep down directions respectively.

were etched with 1.5 pA Ga ion current as schematically shown in the inset of Fig. 1. Two nominally identical JJs as shown in Fig. 1 with lateral dimension of  $0.12 \mu\text{m}^2$  were fabricated in each arm of the SQUID loop.

I-V characteristics of the DC SQUIDS with different Al barrier thickness and oxidation conditions were measured at 4.2 K and the parameters of these devices are tabulated in table 1. The critical current of the SQUID decreased from 750 to  $25 \mu\text{A}$  with the increase in the oxygen exposure time. As the fabricated JJs are of similar size the observed behavior is due to the decrease in the critical current density ( $J_a$ ) of the junction with the increases in the oxygen exposure time, which determines the  $\text{AlO}_x$  barrier thickness. The hysteresis present in the devices having relatively thin  $\text{AlO}_x$  barrier thickness is removed with the increases in the oxygen exposure time. The current density of the junctions increased with the reduction in the Al barrier thickness as observed in SQUID DS-E. In all the DC SQUIDS except DS-B and DS-D, we have fabricated 6 identical SQUIDS and the mean value of  $I_c$  is tabulated in the table.1. The  $I_c$  of the DC SQUIDS was found to be highly reproducible with less than  $\pm 6\%$  variation from the mean value.

Figure 2 shows the current-voltage (I-V) characteristics of a DC SQUID (DS-A) measured at 4.2 K. The I-V curve shows that the SQUID is hysteretic with a critical current ( $I_c$ ) of  $750 \mu\text{A}$ . The hysteretic behavior of the SQUID indicates that the junctions are underdamped [12]. During the FIB sidewall etching, the Ga ions implanted into the sidewalls suppress the superconductivity of Nb up to a thickness of about 30 nm, as estimated using simulation by Troeman *et al.* [6]. To avoid any contribution to the  $I_c$  of the tunnel junction from this Ga implanted sidewall, they were passivated using standard anodization process [13]. DC SQUIDS were anodized at constant potential of 40 V for 60 s in an electrolytic solution containing 165 g ammonium pentaborate, 1120 ml ethylene glycol and 760 ml deionized water. Figure 2 shows the I-V characteristic of the DC SQUID after anodization (DS-B), which resulted in reduction of the  $I_c$

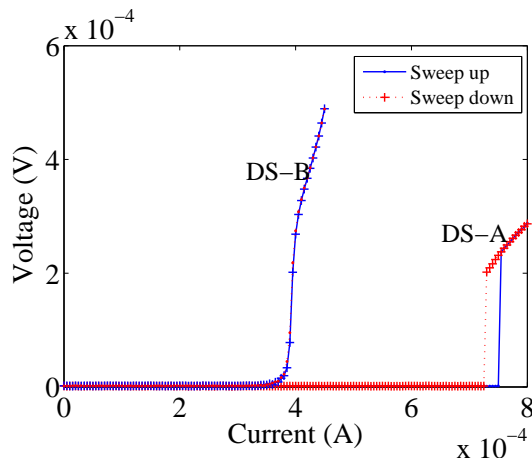


FIG. 2: The I-V characteristic of the as-fabricated (DS-A) and anodized (DS-B) Nb/Al( $\text{AlO}_x$ )/Nb DC SQUIDS measured at 4.2 K.

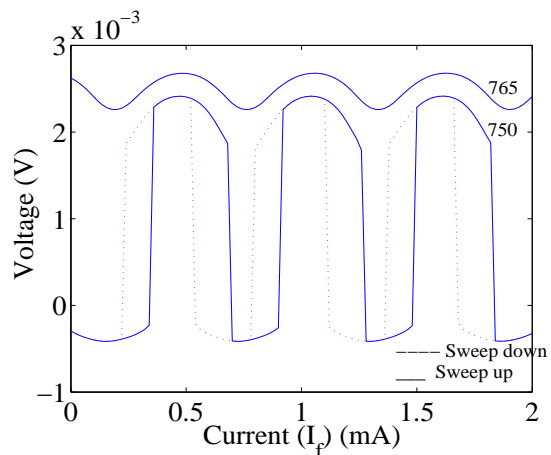


FIG. 3: Flux response of the hysteretic (DS-A) DC SQUID measured for  $I_b$  of 750 and  $765 \mu\text{A}$  in sweep up and sweep down directions.

of the SQUID from 750 to  $390 \mu\text{A}$ , and in the elimination of the hysteretic behavior. The normal state resistance of the junctions determined from the I-V increased from 1 to  $4.8 \Omega$  after anodization.

The flux response of the hysteretic (DS-A) and non-hysteretic (DS-B) DC SQUIDS were measured at 4.2 K. In this measurement the modulation in the voltage across the SQUID was recorded as a function of the current applied to the magnetic flux lines ( $I_f$ ) and SQUID bias current ( $I_b$ ). The flux response of the hysteretic SQUID was measured from  $I_f = 0 \text{ mA}$  to 2 mA in steps of 0.02 mA both in sweep up and sweep down directions. This measurement was repeated for SQUID bias current  $I_b$  of 750 and  $765 \mu\text{A}$  (see Fig. 3). For  $I_b$  of  $750 \mu\text{A}$  the voltage across the SQUID is highly modulated and measured voltage is asymmetric function of flux both in the

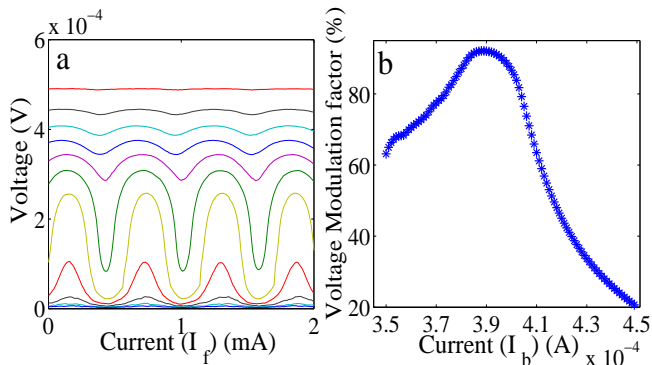


FIG. 4: (a) Flux response of a non-hysteretic (DS-B) DC SQUID measured at different SQUID bias current ( $I_b$ ) from 350 to 450  $\mu\text{A}$  in steps of 10  $\mu\text{A}$ . (b) Plot of voltage modulation factor as a function of SQUID bias current ( $I_b$ ).

sweep up and down directions as shown in Fig. 3. The voltage modulation factor of the SQUID calculated using  $((V_{\text{max}} - V_{\text{min}})/V_{\text{max}}) \times 100\%$  in this region is found to be 96% (where  $V_{\text{max}}$  and  $V_{\text{min}}$  are respectively the maximum and minimum voltage measured with respect to the flux changes). The flux response curve becomes symmetric and the modulation factor decreases to 19% at  $I_b$  of 765  $\mu\text{A}$  and the flux response curve for the sweep up and down direction become identical as shown in Fig. 3.

The flux response of the non-hysteretic DC SQUID (DS-B) is shown in Fig. 4a. This SQUID did not exhibit flux sensitivity for  $I_b$  below 350  $\mu\text{A}$  and above 450  $\mu\text{A}$ , and showed periodic modulation of the voltage within this range as shown in Fig. 4a. In this non-hysteretic SQUID no switching like behavior is observed and the voltage is rather smooth and symmetric with respect to  $V_{\text{max}}$  with relatively high modulation depth. The flux response curves of this SQUID are identical irrespective of the direction of the  $I_f$  sweep and hence the flux response

with respect to sweep up direction is only plotted here. The calculated modulation factor is plotted against  $I_b$  in Fig. 4b. The modulation factor increased from 60% at  $I_b$  of 350  $\mu\text{A}$  and reached a maximum value of 92% at  $I_b$  of 392  $\mu\text{A}$ . After reaching the maximum the modulation factor gradually decreases with the further increase in  $I_b$  as shown in Fig. 4b. The relatively high modulation factor indicates that the two JJs of the SQUID have similar critical currents, demonstrating thus the good repeatability of the FIB fabrication technique.

The operation of the DC SQUID (DS-A) was tested from 4.2K down to 0.1K. The critical current of the junction increased from 750  $\mu\text{A}$  at 4.2K to 1880  $\mu\text{A}$  at 0.1K. The flux response of this SQUID measured at 0.1K had shown periodic voltage modulation with a modulation factor of 80%. These results demonstrate that DC SQUIDS fabricated in the present process have very high modulation factor over a wide range of temperatures compared to the DC SQUIDS made of Nb nanobridges.

In summary, Nb/Al(AIO $x$ )/Nb DC SQUIDS with nanoscale JJs were successfully fabricated using relatively simple process consisting of a single photolithography step and a single 3D FIB etching step. Using this process hysteretic and non-hysteretic DC SQUIDS were fabricated by varying the Al barrier thickness and oxidation conditions. Hysteretic SQUIDS exhibited asymmetric flux response curve with high modulation factor. Non-hysteretic SQUIDS have shown smooth symmetric flux response, and the voltage modulation factor in this case reached a maximum value of 92% near the critical current of the SQUID.

D. Yuvaraj is supported by the Viterbi fellowships. This work is supported by the German Israel Foundation under grant 1-2038.1114.07, the Israel Science Foundation under grant 1380021, the Deborah Foundation, Russell Berrie Nanotechnology Institute, the European STREP QNEMS Project, Israeli ministry of science and MAFAT.

- 
- [1] J. Clarke and A. I. Braginski, *The SQUID Handbook: Fundamentals and Technology of SQUIDS and SQUID Systems* (Wiley-VCH, 2004), 1st ed., ISBN 3527402292.
- [2] S. Etaki, M. Poot, I. Mahboob, K. Onomitsu, H. Yamaguchi, and H. S. J. van der Zant, *Nat. Phys.* **4**, 785 (2008), ISSN 1745-2473.
- [3] J. Lee, W. Oliver, T. Orlando, and K. Berggren, *IEEE Transactions on Applied Superconductivity* **15**, 841 (2005).
- [4] A. Finkler, Y. Segev, Y. Myasoedov, M. L. Rappaport, L. Ne.Eman, D. Vasyukov, E. Zeldov, M. E. Huber, J. Martin, and A. Yacoby, *Nano Lett.* **10**, 1046 (2010).
- [5] S. Morohashi, F. Shinoki, A. Shoji, M. Aoyagi, and H. Hayakawa, *Appl. Phys. Lett.* **46**, 1179 (1985).
- [6] A. Troeman, H. Derking, B. Borger, J. Pleikies, D. Veldhuis, and H. Hilgenkamp, *Nano Lett.* **7**, 2152 (2007), ISSN 1530-6984.
- [7] K. Hasselbach, D. Maily, and J. Kirtley, *J. Appl. Phys.* **91**, 4432 (2002).
- [8] E. Segev, O. Suchoi, O. Shtempluck, F. Xue, and E. Buks, *Phys. Rev. B* **83**, 104507 (2011).
- [9] C. Bell, G. Burnell, D.-J. Kang, R. H. Hadfield, M. J. Kappers, and M. G. Blamire, *Nanotechnology* **14**, 630 (2003).
- [10] K. Matsuba, M. Watanabe, and J. Tsai, *J. Appl. Phys.* **103**, 074303 (2008).
- [11] M. Watanabe, Y. Nakamura, and J.-S. Tsai, *Appl. Phys. Lett.* **84**, 410 (2004).
- [12] J. M. Kivioja, T. E. Nieminen, J. Claudon, O. Buisson, F. W. J. Hekking, and J. P. Pekola, *New J. Phys.* **7**, 179 (2005).
- [13] H. Kroger, L. N. Smith, and D. W. Jillie, *Appl. Phys.*

Lett. **39**, 280 (1981).